

VID-Fusion: Robust Visual-Inertial-Dynamics Odometry for Accurate External Force Estimation

Ziming Ding, Tiankai Yang, Kunyi Zhang, Chao Xu and Fei Gao

Abstract—Recently, quadrotors are gaining significant attention in aerial transportation and delivery. In these scenarios, an accurate estimation of the external force is as essential as the 6 degree-of-freedom (DoF) pose since it is of vital importance for planning and control of the vehicle. To this end, we propose a tightly-coupled Visual-Inertial-Dynamics (VID) system that simultaneously estimates the external force applied to the quadrotor along with the 6 DoF pose. Our method builds on the state-of-the-art optimization-based Visual-Inertial system [1], with a novel deduction of the dynamics and external force factor extended from VIMO [2]. Utilizing the proposed dynamics and external force factor, our estimator robustly and accurately estimates the external force even when it varies widely. Moreover, since we explicitly consider the influence of the external force, when compared with VIMO [2] and VINS-Mono [1], our method shows comparable and superior pose accuracy, even when the external force ranges from neglectable to significant. The robustness and effectiveness of the proposed method are validated by extensive real-world experiments and application scenario simulation. We will release an open-source package of this method along with datasets with ground truth force measurements for the reference of the community.

I. INTRODUCTION

Micro Aerial Vehicles (MAVs), especially quadrotors, have long been paying expectancy in package delivery, aerial manipulation, and collaborative transportation. In these applications, quadrotors are required to carry heavy payloads or suspended cargoes, which applies external forces periodically to the drone. These forces are un-neglectable, thus causing large disturbances and significantly harming the flight of the quadrotor. To compensate for the disturbances, the controller and planner of a quadrotor have to precisely know the magnitude and direction of the external force in advance. Therefore, it is necessary and urgent to design a state estimator, which takes external forces into explicit consideration.

Recently, the Visual Inertial Odometry (VIO) [1, 3] system has shown its reliable capability to provide robust and accurate state estimation of a quadrotor, even within the minimalist hardware configuration, such as a monocular or stereo camera with an inertial measurement unit (IMU). To combine the external disturbance force estimation into a VIO system, VIMO [2] formulates a model-based VIO in a tightly coupled manner [1] and opens the door to simultaneously estimate motion and external forces with a VIO system. By considering the dynamics model of the quadrotor as a new information source, VIMO improves the accuracy of pose

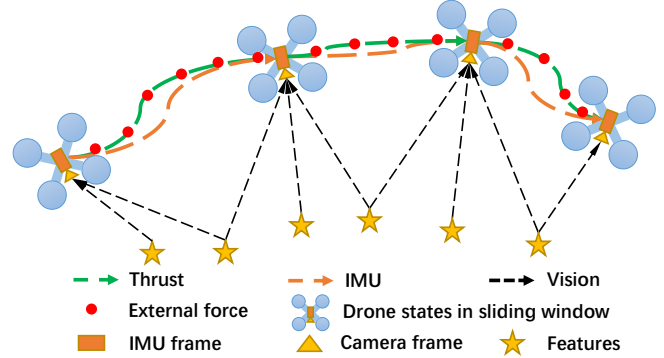


Fig. 1: The thrust, external force observation and IMU measurements in the sliding windows. The combination of thrust and external force contributes equally to IMU measurements in theory. Moreover, the thrust and external force will be added into the sliding window processing to formulate the model-based visual-inertial force estimation framework.

estimation and utilizes the dynamics to provide a clue for the external force estimation. VIMO [2] jointly estimates the motion and forces by modeling the unknown external forces as zero-mean Gaussian values, assuming the external forces estimated is near zero or only occurs in a short period. Obviously, this assumption only holds for narrow scenarios and results in severe instability or even failure to pose estimation when the drone receives large or continuous forces.

To accurately model and measure the effects of external forces, it is necessary to incorporate the quantification of external force into a VIO system. As illustrated in Fig. 1, the external force is roughly equal to the discrepancy between motions measured from IMU and thrust measurements without considering sensor noise characteristics. In this paper, instead of using the zero-mean Gaussian assumption, we provide a rough force observation by comparing IMU and thrust. We derive an external force preintegration term to represent the average force between consecutive camera frames and then combine the thrust preintegration proposed in [2] to reformulate the dynamics residual. Finally, the stacked residual is jointly minimized by using nonlinear optimization.

In this paper, we improve the force estimation based on the model-based VIO [2] and propose an optimization-based Visual-Inertial-Dynamics (VID) framework extended from [1, 3, 4]. Compared with VIMO [2] and VINS-Mono [1], the proposed estimator demonstrates superior pose and force estimation accuracy and attains robustness even when the external force varies widely.

To summarize our contributions:

- We derive the external force preintegration and propose state, covariance propagation, and force bias correction for discrete-time processing.
- We incorporate the external force preintegration into the state-of-the-art VIO framework and present a complete, robust, tightly-coupled Visual-Inertial-Dynamics state estimator.
- We demonstrate robust and accurate external force and pose estimation onboard the quadrotor and present a new dataset with ground truth measurements.

The rest of the paper is organized as follows. We describe some related works in Sec.II. We model the dynamics-based estimation problem in detail in Sec.III. Following several experiments and an application in Sec.IV, we show the performance of algorithms in this article. Finally, we give relevant conclusions on our algorithm and future work in Sec.V.

II. RELATED WORKS

A. System model and identification

For better external force estimation, we must distinctly comprehend the source of the driven force of a MAVs. [5] describes an online Kalman filter-based method to identify a quadrotor system, especially geometrical and inertial parameters. However, dynamics parameters such as the thrust coefficient still need to be measured by experiments. In [6], the authors give us almost all the details corresponding to a multi-copter system, but it demands offline experiments with a specialized device to obtain the relation between rpm and aerodynamic force, including thrust.

B. Motion state estimation

Before disturbance estimation, the motion state is the hot spot in the relevant field. Especially, visual-inertial odometry has achieved a lot of excellent achievements and extensive applications. MSCKF [7], VINS-Mono [1], OpenVINS [8] and so on are some brilliant open-source works. All algorithms above work well in most conditions due to effective, robust and online features, but they neglect the robot's dynamics, focusing only on the ego-motion state estimation with as little as possible sensors. So in complex environments [9]–[11] with contacts, interactions and disturbances, we can not achieve an ideal goal only with an unreliable setting value of disturbance.

C. External force estimation

Actually, We could derive from subtracting the collective thrust from the inertial measurements [12] if knowing the exact force at any moment. Or, a nonlinear observer such as [13]–[15] is plausible as if we have a good dynamics model and enough measurements. Also, some filter-based method is quite effective due to its feature of filtering noise. [16]–[19] use a loosely-coupled filter-based method to estimate a disturbance but neglecting the interaction of different sensor data, resulting in a draft or bias of the estimator. VIMO [2] bridges the gap between motion estimation and

external force estimation within a VIO system. Although it is an optimization-based method, it utilizes a sliding window technique to smooth the systemically estimated state, including external force. However, within a monocular camera, IMU, and an additional thrust of a MAV, VIMO [2] jointly estimates the motion and external forces by modeling the unknown external force as a zero-mean Gaussian value in a tightly coupled framework [1]. So, the external forces actually exerted on VIMO should be neglectable or only last shortly. Otherwise, the estimator will be highly affected and even leads to failure of the system by large or continuous forces such as loads on multi-rotors. So the external force should be quantified by modeling the effects on motion, guaranteeing the robustness of model-based visual-inertial odometry at the same time.

III. METHODOLOGY

A. External Force Preintegration

We formulate our external force preintegration inspired by acceleration preintegration in [20] and [4], and extend preintegration of dynamics factor in [2] to be a dynamics and external force preintegration factor.

1) *External Force Quantification*: The quantification of the external force exerted on a drone needs to combine accelerometer data from inertial measurement unit (IMU) and the rotor thrust from the rotor rotating speed measurement unit (RMU), in which the raw acceleration $\hat{\mathbf{a}}^b$ and the mass normalized thrust acceleration $\hat{\mathbf{T}}^b$ is modeled as:

$$\begin{aligned}\hat{\mathbf{a}}^b &= \mathbf{a}^b + \mathbf{b}_a + \mathbf{R}_w^b \mathbf{g}^w + \mathbf{n}_a \\ \hat{\mathbf{T}}^b &= \frac{1}{m} \sum_{i=1}^{n_{rotor}} (\tau_{fi} \omega_i^2) + \mathbf{n}_T,\end{aligned}\quad (1)$$

where the noise of acceleration and thrust measurements are assumed as Gaussian white noise:

$$\mathbf{n}_a \sim \mathcal{N}(\mathbf{0}, \sigma_a^2), \quad \mathbf{n}_T \sim \mathcal{N}(\mathbf{0}, \sigma_T^2). \quad (2)$$

\mathbf{a}^b is true value of acceleration in IMU frame and \mathbf{b}_a is the acceleration measurement bias, whose derivative is also assumed as Gaussian white noise with

$$\dot{\mathbf{b}}_a = \mathbf{n}_{b_a}, \quad \mathbf{n}_{b_a} \sim \mathcal{N}(\mathbf{0}, \sigma_{b_a}^2). \quad (3)$$

\mathbf{R}_w^b is the rotation matrix from the world frame to the time-varying body frame, provided by the gyroscope of IMU $\dot{\mathbf{q}}_b^w = \mathbf{q}_b^w \otimes [0, \boldsymbol{\omega}^b \Delta t]^T$, where \otimes is the quaternion multiplication and $\boldsymbol{\omega}^b$ is the body angular velocity in body frame, and the gyroscope measurements with noise and bias from IMU is

$$\hat{\boldsymbol{\omega}}^b = \boldsymbol{\omega}^b + \mathbf{b}_\omega + \mathbf{n}_\omega, \quad (4)$$

\mathbf{n}_ω and the derivative of \mathbf{b}_ω are also considered as Gaussian white noise:

$$\dot{\mathbf{b}}_\omega = \mathbf{n}_{b_\omega}, \quad \mathbf{n}_{b_\omega} \sim \mathcal{N}(\mathbf{0}, \sigma_{b_\omega}^2), \quad \mathbf{n}_\omega \sim \mathcal{N}(\mathbf{0}, \sigma_\omega^2). \quad (5)$$

The gravity vector is $\mathbf{g}^w = [0, 0, -9.79]m/s^2$. Besides, m stands for mass, and n_{rotor} stands for the number of rotors,

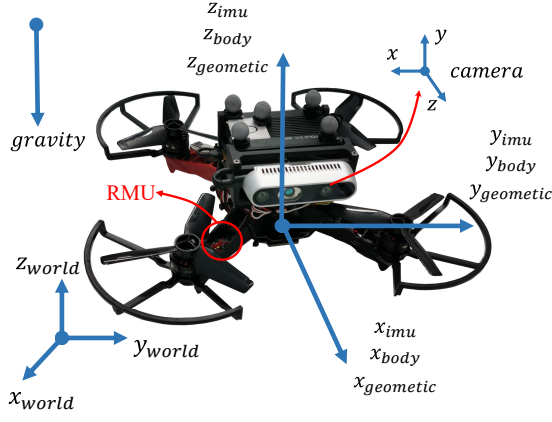


Fig. 2: The frames defined in our system, where body frame, IMU frame and geometric frame is assumed coincided.

and τ_{f_i} is thrust coefficient for i th rotor of any arbitrary multi-rotors, and ω_i is the i th rotor rotation speed from RMU. More details and system identification about thrust coefficient will be discussed in III-C. Here, we assume that the IMU frame is the body frame, and the geometric center of the drone is coincident with the drone centroid and IMU center. They are all called the body frame in our framework. We consider external force as a resultant force except for rotor thrust and aircraft gravity, acting on the mass center. So we can derive the relationship between $\hat{\mathbf{a}}^b$ and $\hat{\mathbf{T}}^b$:

$$\begin{aligned} \mathbf{a}^b &= \hat{\mathbf{T}}^b + \mathbf{f}_{ex}^b - \mathbf{R}_w^b \mathbf{g}^w - \mathbf{n}_T \\ &= \hat{\mathbf{a}}^b - \mathbf{b}_a - \mathbf{R}_w^b \mathbf{g}^w - \mathbf{n}_a. \end{aligned} \quad (6)$$

\mathbf{f}_{ex}^b represents external force theoretically calculated at any time in body frame. And now we can calculate external force with simple operation as follow:

$$\mathbf{f}_{ex}^b = (\hat{\mathbf{a}}^b - \mathbf{b}_a - \hat{\mathbf{T}}^b) - (\mathbf{n}_a - \mathbf{n}_T). \quad (7)$$

2) *Preintegration*: The external force \mathbf{f}_{ex}^b calculated from (7) have same dimension as acceleration expressed in body frame, so we are inspired by acceleration measurement preintegration method to integrate external force between key frames b_k and b_{k+1} and represent it at frame b_k :

$$\hat{\mathbf{J}}_{b_{k+1}}^{b_k} = \int_{t_k}^{t_{k+1}} \mathbf{R}_{b_\tau}^{b_k} \mathbf{f}_{ex}^{b_\tau} d\tau \quad (8)$$

$$\hat{\mathcal{F}}_{b_{k+1}}^{b_k} = \frac{1}{\Delta t_k} \hat{\mathbf{J}}_{b_{k+1}}^{b_k}. \quad (9)$$

$\hat{\mathbf{J}}_{b_{k+1}}^{b_k}$ represents the integration of external force over time interval $\Delta t_k = t_{k+1} - t_k$ referencing frame b_k . Then we use $\hat{\mathcal{F}}_{b_{k+1}}^{b_k}$ to represent the average force between frames b_k and b_{k+1} . During $[t_k, t_{k+1}]$, $\hat{\mathcal{F}}_{b_{k+1}}^{b_k}$ can be considered as a constant force exerting in b_k frame. $\mathbf{R}_{b_\tau}^{b_k}$ is provided by the integration of rotation $\hat{\gamma}_{b_\tau}^{b_k}$, which will be mentioned in (11).

3) *External Force Preintegration*: We add external force preintegration derived above into preintegration of dynamics

factor in [2], and adjust to 3 preintegration terms containing measurements: $\hat{\alpha}_{b_{k+1}}^{b_k}$, $\hat{\beta}_{b_{k+1}}^{b_k}$, $\hat{\mathcal{F}}_{b_{k+1}}^{b_k}$. These terms are integrated from IMU and thrust measurements expressed in frame b_k , which are independent of the world frame.

$$\begin{aligned} \hat{\alpha}_{b_{k+1}}^{b_k} &= \iint_{t_k}^{t_{k+1}} \mathbf{R}_{b_\tau}^{b_k} (\hat{\mathbf{T}}^{b_\tau} - \mathbf{n}_T) d\tau^2 \\ \hat{\beta}_{b_{k+1}}^{b_k} &= \int_{t_k}^{t_{k+1}} \mathbf{R}_{b_\tau}^{b_k} (\hat{\mathbf{T}}^{b_\tau} - \mathbf{n}_T) d\tau \\ \hat{\mathcal{F}}_{b_{k+1}}^{b_k} &= \frac{1}{\Delta t_k} \int_{t_k}^{t_{k+1}} \mathbf{R}_{b_\tau}^{b_k} \mathbf{f}_{ex}^{b_\tau} d\tau. \end{aligned} \quad (10)$$

$\hat{\alpha}_{b_{k+1}}^{b_k}$ represents the contribution to distance by the thrust during $[t_k, t_{k+1}]$, $\hat{\beta}_{b_{k+1}}^{b_k}$ represents the velocity contributed by thrust, and $\hat{\mathcal{F}}_{b_{k+1}}^{b_k}$ represents the average external force in the period.

4) *External Force Propagation*: As for discrete-time processing, we employ first-order hold numerical integration method as done in [1]. In the period of $[t_k, t_{k+1}]$, every initial value $\hat{\alpha}_{b_k}^{b_k}, \hat{\beta}_{b_k}^{b_k}$ of propagation at t_k is set to $\mathbf{0}$. At the period of $[t_k, t_{k+1}]$, the external force $\hat{\mathcal{F}}_{b_k}^{b_k}$ propagates in the same way as $\hat{\alpha}_{b_k}^{b_k}$ and $\hat{\beta}_{b_k}^{b_k}$. At the moment of t_{k+1} , $\hat{\mathcal{F}}_{b_{k+1}}^{b_k}$ will be divided by Δt_k , calculating average force in the time interval $[t_k, t_{k+1}]$. There is a requirement of rotation matrix $\mathbf{R}_i^{b_k}$ during propagation, so quaternion preintegration $\hat{\gamma}_i^{b_k}$ is employed to propagate from frame b_k to current timestamp t_i of IMU measurements with initial state of identity quaternion. During propagation period $[t_k, t_{k+1}]$, the biases of acceleration and gyroscope measurements are considered as constant value, the estimated result at time t_k are b_{a_k} and b_{ω_k} respectively.

$$\begin{aligned} \hat{\alpha}_{i+1}^{b_k} &= \hat{\alpha}_i^{b_k} + \hat{\beta}_i^{b_k} \delta t_i + \frac{1}{2} \mathbf{R}_i^{b_k} \hat{\mathbf{T}}^{b_i} \delta t_i^2 \\ \hat{\beta}_{i+1}^{b_k} &= \hat{\beta}_i^{b_k} + \mathbf{R}_i^{b_k} \hat{\mathbf{T}}^{b_i} \delta t_i \\ \hat{\mathcal{F}}_{i+1}^{b_k} &= \hat{\mathcal{F}}_i^{b_k} + \mathbf{R}_i^{b_k} (\hat{\mathbf{a}}^{b_i} - \mathbf{b}_{a_k} - \hat{\mathbf{T}}^{b_i}) \delta t_i \\ \hat{\gamma}_{i+1}^{b_k} &= \hat{\gamma}_i^{b_k} \otimes \left[\frac{1}{2} (\boldsymbol{\omega}^{b_i} - \mathbf{b}_{\omega_k}) \delta t_i \right], \end{aligned} \quad (11)$$

where δt_i is time interval between two continuous IMU measurements i and $i+1$. Here, $\hat{\mathbf{T}}^{b_i}$ updates at the rate of RMU, while $\hat{\mathbf{a}}^{b_i}$ and $\boldsymbol{\omega}^{b_i}$ at IMU rate. Propagation runs at the faster measurement rate. When the faster measurement update, the slower one will keep the latest measurement and both of them will be propagated together.

As for propagation in $[t_k, t_{k+1}]$, the error state $\delta \mathbf{z} = [\delta \boldsymbol{\alpha}^T \delta \boldsymbol{\beta}^T \delta \mathcal{F}^T \delta \mathbf{b}_a^T \delta \mathbf{b}_\omega^T]^T$ and the state covariance matrix $\mathbf{P}_i^{b_k}$ will be propagated by a linearized model with initialization of $\delta \mathbf{z}_{b_k}^{b_k} = \mathbf{0}, \mathbf{P}_{b_k}^{b_k} = \mathbf{0}$, while the first-order Jacobian matrix \mathbf{J}_i of $\mathbf{z}_i^{b_k}$ with respect to $\mathbf{z}_{b_k}^{b_k}$ can be also propagated with initialization of $\mathbf{J}_{b_k} = \mathbf{I}$:

$$\delta \mathbf{z}_{i+1}^{b_k} = \mathbf{F}_i \delta \mathbf{z}_i^{b_k} + \mathbf{G}_i \mathbf{n}, \quad (12)$$

$$\mathbf{P}_{i+1}^{b_k} = \mathbf{F}_i \mathbf{P}_i^{b_k} \mathbf{F}_i^T + \mathbf{G}_i \mathbf{Q} \mathbf{G}_i^T, \quad (13)$$

$$\mathbf{J}_{i+1} = \mathbf{F}_i \mathbf{J}_i, \quad (14)$$

where \mathbf{F}_i is the linearized state-transition matrix of the error state, while \mathbf{n} is the noise vector $\mathbf{n} = [\mathbf{n}_T^T \mathbf{n}_\omega^T \mathbf{n}_{b_\omega}^T \mathbf{n}_a^T \mathbf{n}_{b_a}^T]^T$, and \mathbf{G}_i is the noise matrix of the error state. Using the recursive propagation method, we can get the covariance matrix $\mathbf{P}_{b_{k+1}}^{b_k}$ and Jacobian \mathbf{J}_{k+1} at time t_{k+1} .

5) *Bias Correction*: As we propagate $\hat{\alpha}_{b_{k+1}}^{b_k}, \hat{\beta}_{b_{k+1}}^{b_k}, \hat{\mathcal{F}}_{b_{k+1}}^{b_k}$ with an assumption that the biases b_{a_k}, b_{ω_k} are constant, a approximate correction will be employed when the bias changes slightly:

$$\begin{aligned}\hat{\alpha}_{b_{k+1}}^{b_k} &\approx \hat{\alpha}_{b_{k+1}}^{b_k} + \mathbf{J}_{b_\omega}^\alpha \delta b_{\omega_k} \\ \hat{\beta}_{b_{k+1}}^{b_k} &\approx \hat{\beta}_{b_{k+1}}^{b_k} + \mathbf{J}_{b_\omega}^\beta \delta b_{\omega_k} \\ \hat{\mathcal{F}}_{b_{k+1}}^{b_k} &\approx \hat{\mathcal{F}}_{b_{k+1}}^{b_k} + \frac{1}{\Delta t_k} (\mathbf{J}_{b_a}^\mathcal{F} \delta b_{a_k} + \mathbf{J}_{b_\omega}^\mathcal{F} \delta b_{\omega_k}),\end{aligned}\quad (15)$$

where $\mathbf{J}_{b_\omega}^\alpha, \mathbf{J}_{b_\omega}^\beta, \mathbf{J}_{b_a}^\mathcal{F}, \mathbf{J}_{b_\omega}^\mathcal{F}$ are the corresponding block in Jacobian \mathbf{J}_{k+1} . And $\delta b_{\omega_k}, \delta b_{a_k}$ are the bias variations between the initial estimated state and the latest estimated state in t_k of gyroscope and acceleration respectively.

B. Tightly Coupled VIO with External Force Estimation

We employ a sliding window-based tightly-coupled VIO framework as in VINS-Mono [1] and VIMO [2].

1) *System Formulation*: In the sliding window, the full state of the optimization is defined as following:

$$\begin{aligned}\mathcal{X} &= [\mathbf{x}_0, \mathbf{x}_1, \dots, \mathbf{x}_n, \lambda_0, \lambda_1, \dots, \lambda_m], \\ \mathbf{x}_k &= [\mathbf{p}_{b_k}^w, \mathbf{v}_{b_k}^w, \mathbf{q}_{b_k}^w, \mathbf{b}_a, \mathbf{b}_\omega, \mathbf{F}_{ex}^{b_k}], \quad k \in [0, n],\end{aligned}\quad (16)$$

where \mathbf{x}_k is the body state at the k th key frame time with composition of position $\mathbf{p}_{b_k}^w$, velocity $\mathbf{v}_{b_k}^w$, orientation represented in Hamilton quaternion $\mathbf{q}_{b_k}^w$, IMU measurement bias $\mathbf{b}_a, \mathbf{b}_\omega$, and the average external force $\mathbf{F}_{ex}^{b_k}$ in body frame during $[t_k, t_{k+1}]$. Here, n is the size of the sliding window, m is the total number of features in the sliding window, and λ_l is the inverse depth of the l th feature from its first observation in the sliding window as in [1].

In order to obtain the maximum posterior estimation of all residuals concerning \mathcal{X} , we employ the nonlinear optimization problem formulation in [1] and its extension, which considers the dynamics residual in [2]. Crucially, we reformulate the dynamics residual in [2] by using our proposed external force preintegration. The cost function is:

$$\min_{\mathcal{X}} \left\{ \|\mathbf{r}_p\|^2 + \sum_{k \in \mathcal{B}} \|\mathbf{r}_B^k\|_{\mathbf{W}_B^k}^2 + \sum_{(l,j) \in \mathcal{C}} \rho(\|\mathbf{r}_C^{l,j}\|_{\mathbf{W}_C^{l,j}}^2) + \underbrace{\sum_{k \in \mathcal{D}} \left\| \mathbf{r}_D^k \left(\mathbf{x}_k, \mathbf{x}_{k+1}, \hat{\mathbf{z}}_{b_{k+1}}^{b_k} \right) \right\|_{\mathbf{W}_D^k}^2}_{\text{the external force residual}} \right\}, \quad (17)$$

where the first three residuals are the VIO residual terms of prior residual, the sum of the inertial residuals, and the sum of visual residuals with robust core functions, which can be found in more details in [1], the last one is the sum of

Mahalanobis norm of our proposed external force residual, in which, \mathcal{D} is the set of thrust and external force measurements in the sliding window. \mathbf{W}_D^k is the weight matrix of Mahalanobis norm for the k th state in the sliding window. \mathbf{r}_D^k is the corresponding residual at t_k which considers the state $\mathbf{x}_k, \mathbf{x}_{k+1}$ and external force preintegration $\hat{\mathbf{z}}_{b_{k+1}}^{b_k}$.

2) *External Force Residual*: We combine $\hat{\alpha}_{b_{k+1}}^{b_k}, \hat{\beta}_{b_{k+1}}^{b_k}, \hat{\mathcal{F}}_{b_{k+1}}^{b_k}$, the the prediction of preintegration term $\hat{\alpha}_{b_{k+1}}^{b_k}, \hat{\beta}_{b_{k+1}}^{b_k}, \hat{\mathcal{F}}_{b_{k+1}}^{b_k}$ in (10), to formulate our proposed residual between frame b_k and b_{k+1} .

$$\mathbf{r}_D^k \left(\mathbf{x}_k, \mathbf{x}_{k+1}, \hat{\mathbf{z}}_{b_{k+1}}^{b_k} \right) = \begin{bmatrix} \alpha_{b_{k+1}}^{b_k} - \hat{\alpha}_{b_{k+1}}^{b_k} \\ \beta_{b_{k+1}}^{b_k} - \hat{\beta}_{b_{k+1}}^{b_k} \\ \mathcal{F}_{b_{k+1}}^{b_k} - \hat{\mathcal{F}}_{b_{k+1}}^{b_k} \\ \mathbf{b}_{a_{k+1}} - \mathbf{b}_{a_k} \end{bmatrix}, \quad \mathbf{W}_D^k = \mathbf{P}_{b_{k+1}}^{b_k-1}, \quad (18)$$

where

$$\begin{aligned}\alpha_{b_{k+1}}^{b_k} &= \mathbf{R}_w^{b_k} \left(\mathbf{p}_{b_{k+1}}^w - \mathbf{p}_{b_k}^w - \mathbf{v}_{b_k}^w \Delta t_k - \frac{1}{2} \mathbf{g}^w \Delta t_k^2 \right) \\ &\quad - \frac{1}{2} \mathbf{F}_{ex}^{b_{k+1}} \Delta t_k^2 \\ \beta_{b_{k+1}}^{b_k} &= \mathbf{R}_w^{b_k} \left(\mathbf{v}_{b_{k+1}}^w - \mathbf{v}_{b_k}^w - \mathbf{g}^w \Delta t_k \right) - \mathbf{F}_{ex}^{b_{k+1}} \Delta t_k \\ \mathcal{F}_{b_{k+1}}^{b_k} &= \mathbf{F}_{ex}^{b_{k+1}}.\end{aligned}\quad (19)$$

The residual $\delta\alpha, \delta\beta, \delta\mathcal{F}, \delta\mathbf{b}_a$ represents the difference between the prediction model and the measurement integration of the contribution of distance by the thrust, the velocity contributed by thrust, the average force and the measurement bias deviation, respectively. $\hat{\alpha}_{b_{k+1}}^{b_k}, \hat{\beta}_{b_{k+1}}^{b_k}, \hat{\mathcal{F}}_{b_{k+1}}^{b_k}$ are the corrected measurements preintegration in (15). $\mathbf{P}_{b_{k+1}}^{b_k}$ is the weight of Mahalanobis norm which is propagated by (13). As for the other part of the motion state estimation, we use the same marginalization and initialization strategy in [1, 2].

C. On-The-Fly Thrust Coefficient Identification

Since we consider the external force acting on the center of mass and ignoring the disturbance on torque, the system's parameters we need to identify are the mass of the drone and thrust coefficients of the propellers. The mass can be easily obtained, but thrust coefficient identification is often required in the force sensor, which is expensive. Here, we employ a simple online method to estimate the thrust coefficients with a given mass. We consider the centroid and the geometry center are coincident, and each propeller from the quadrotor is equally distributed $mg/4$ gravity when the quadrotor is hovering. Then we estimate the thrust coefficient for each propeller by the Recursive Least Squares method.

IV. RESULTS

In this section, we evaluate our proposed algorithm by real-world experiments and an application focusing on the accuracy and robustness of both odometry and force. We show the accuracy analysis in the experiments and evaluate the proposed algorithm in different scenes: flight without

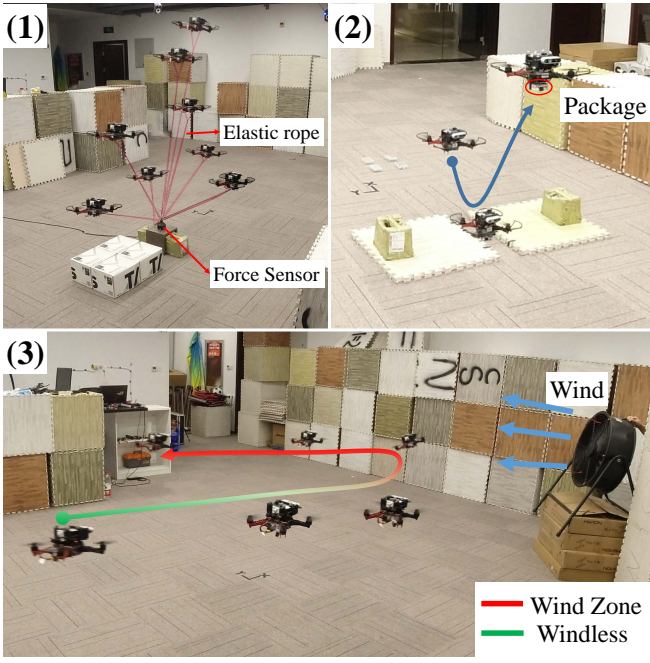


Fig. 3: (1) shows the roped flight experiment, the drone flies with different elasticity. The force estimation compared with VIMO and ground truth is illustrated in Fig. 4. (2) shows the flying scale application, the drone flies down and picks up the package, and the force estimation is illustrated in Fig. 6. (3) shows the flight in wind, the drone is blown away in the red part, and the force estimation will be illustrated in our proposed video.

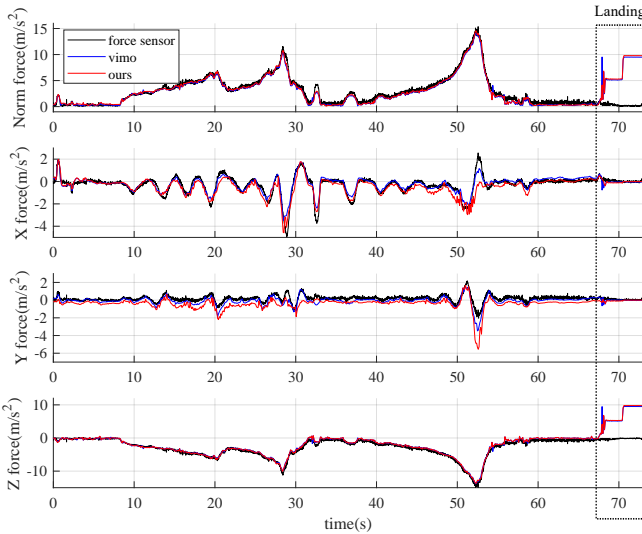


Fig. 4: Force from elastic rope in norm, x , y , z , with RMSE = [0.998, 0.488, 0.751, 0.442]. The drone lands after 66.1s.

loads, flight with loads, flight in wind. And we evaluate the external force estimation with a force sensor. In addition, we simulate the scene of package delivery by drone, where we try to weigh the package in the air like a flying scale.

A. Real-world Experiments

1) *Hardware Setup*: As for validation in real-world experiments, we use the quadrotor platform, as shown in Fig. 2, with an onboard computer (i7-8550U), a stereo camera (Intel

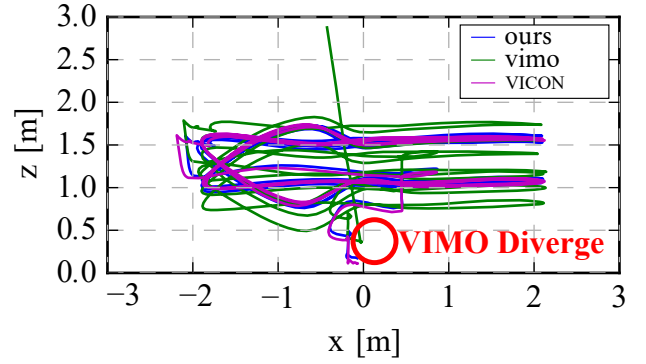


Fig. 5: Trajectories 1 of flight with loads. The odometry estimation of VIMO is affected by the external force from loads, when the drone lands, the external force is the normal force, causing the divergence of VIMO, as illustrated above.

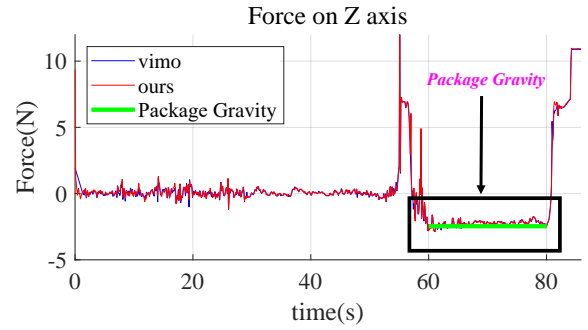


Fig. 6: Force estimation in flying scale experiment. The drone weighs the package during the 60s and 80s. The peak before weighing is the normal force when the drone lands for the package. The RMSE between the gravity of the package and the estimation is about 0.29N.

Realsense D435), a DJI N3 controller providing IMU data. As for the homemade RMU, we use a voltage comparator to measure the changing of rotor phases by an ARM-based micro computing unit (MCU) and then calculate the rotor rpm by fast Fourier transform (FFT) [21]. We obtain the IMU data at 400Hz, imagery data at 30Hz, RMU data at 100Hz. We identify the thrust coefficient for rotors by the proposed method in III-C with a given mass of the drone.

2) *Trajectory Flight*: We record the data from three kinds of flight trajectories: flight without loads, flight with loads fixed on the drone, and flight in wind. The external force of flight without loads is the aerodynamic drag force. And the external force of flight with loads comes from a combination of the gravity and acceleration of the loads and the aerodynamic drag. The last one tests in an scene where the drone tries to fly in front of a fan and is finally blown away by the wind, which is illustrated in Fig. 3 (3). Our algorithm can estimate the external force from wind, which will be shown in the video. VIMO usually fails when the force is unneglectable large especially in landing period, such as shown in Fig. 5. Therefore, results shown in Fig. 7 ~ 8 and TAB. I are only the tests that VIMO does not diverge, for better illustrating the robustness and the accuracy of our proposed VID-Fusion.

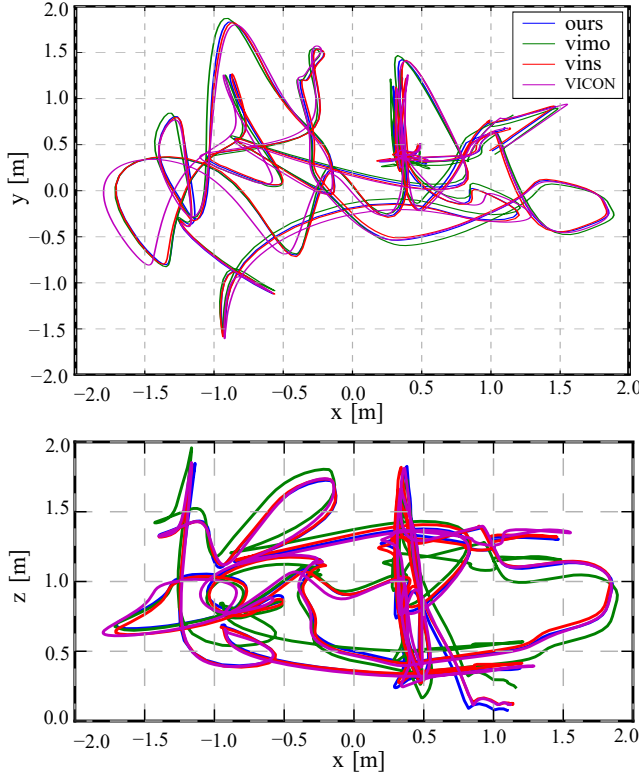


Fig. 7: Trajectories 1 of flight with loads. Ours keeps the accuracy compared with VINS-Mono, while VIMO is strongly affected by the external force, especially z axis.

TABLE I: Real-world Experiment Evaluation

Trajectory	trans. RMSE(m)			rot. RMSE(deg)		
	VINS	VIMO	Ours	VINS	VIMO	Ours
1 w/o loads	0.058	0.058	0.057	4.03	3.36	3.86
2 w/o loads	0.201	0.240	0.198	4.43	4.32	4.84
1 w/ loads	0.132	0.285	0.120	3.37	4.09	3.22
2 w/ loads	0.102	0.239	0.103	4.28	4.40	4.28
In wind	0.091	0.076	0.090	3.81	3.90	3.89
Flying scale	0.069	0.091	0.088	4.44	4.28	4.58

3) *Roped Flight*: To evaluate the estimated force's accuracy, we perform a roped flight test, in which we connect the drone and force sensor by an elastic rope, as shown in Fig. 3 (1). The result shows that our proposed method can provide accurate force estimation whenever the force is slight or large. The external force evaluation is illustrated in Fig. 4.

B. Application

We apply our proposed method in a simulated scene of package delivery as an application of weighing package in the air. As shown in Fig. 3 (3), the drone flies down to attach the package. After taking off again, the drone will weigh the package in the air, hovering, like a flying scale. The force estimation and weighing results are shown in Fig. 6.

According to the odometry estimation shown in Fig. 8 and TAB. I, and the force estimation shown in Fig. 4 and Fig. 6, the proposed VID-Fusion provides a robust and accurate performance on both odometry and external force estimation, even the external force ranges from neglectable to significant.

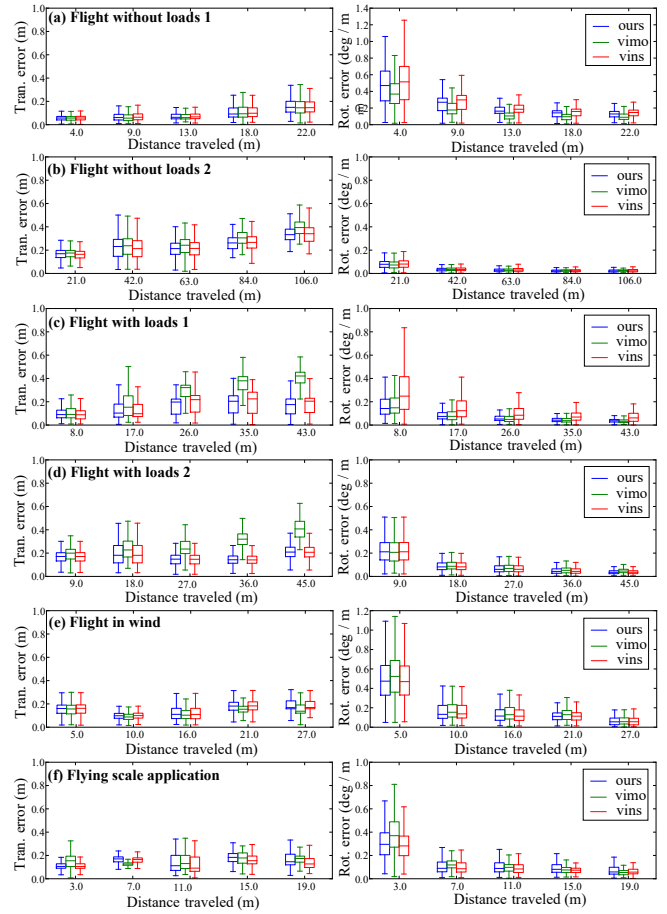


Fig. 8: RMSE of translation and rotation in the proposed experiments. Combining with TAB. I, our proposed algorithm shows similar even better performance with VINS-Mono in different external force situations, while VIMO shows a much worse performance under a large external force.

V. CONCLUSION

This paper proposes an approach that offers robust and accurate odometry for external force estimation based on tightly-coupled optimization-based VIO framework [1]. Our proposed estimator increases the robustness and accuracy in odometry estimation when the force is large or lasts for a long time.

The proposed visual-inertial-dynamics estimator framework can be easily extended into a stereo visual-inertial system such as VINS-Fusion [22], and it can run without model measurements, going back to a VIO system, and the external force will be the combination of normal force and acceleration. Moreover, compared with VINS-Mono [1], we keep the accuracy of odometry estimation and even provide an increase in some scenarios, with an accurate external force estimation additionally. Since we use a simplified dynamics model in this paper, the thrust torque is not yet utilized and is left as our future work. Finally, as a return to the community, the source code and our customized datasets will be released¹.

¹Code, and the dataset will be released after the acceptance of this paper at <https://github.com/ZJU-FAST-Lab/VID-Fusion>

REFERENCES

- [1] T. Qin, P. Li, and S. Shen, “Vins-mono: A robust and versatile monocular visual-inertial state estimator,” *IEEE Transactions on Robotics*, vol. 34, no. 4, pp. 1004–1020, 2018.
- [2] B. Nisar, P. Foehn, D. Falanga, and D. Scaramuzza, “Vimo: Simultaneous visual inertial model-based odometry and force estimation,” *IEEE Robotics and Automation Letters*, vol. 4, no. 3, pp. 2785–2792, 2019.
- [3] S. Leutenegger, S. Lynen, M. Bosse, R. Siegwart, and P. Furgale, “Keyframe-based visual-inertial odometry using nonlinear optimization,” *The International Journal of Robotics Research*, vol. 34, no. 3, pp. 314–334, 2015.
- [4] C. Forster, L. Carlone, F. Dellaert, and D. Scaramuzza, “On-manifold preintegration for real-time visual-inertial odometry,” *IEEE Transactions on Robotics*, vol. 33, no. 1, pp. 1–21, 2016.
- [5] V. Wuest, V. Kumar, and G. Loianno, “Online estimation of geometric and inertia parameters for multirotor aerial vehicles,” 05 2019, pp. 1884–1890.
- [6] Q. Quan, *Introduction to Multicopter Design and Control*. Springer Singapore, 2017.
- [7] M. Li and A. I. Mourikis, “High-precision, consistent ekf-based visual-inertial odometry,” *The International Journal of Robotics Research*, vol. 32, no. 6, pp. 690–711, 2013.
- [8] P. Geneva, K. Eickenhoff, W. Lee, Y. Yang, and G. Huang, “Opencvins: A research platform for visual-inertial estimation,” in *2020 IEEE International Conference on Robotics and Automation (ICRA)*. IEEE, 2020, pp. 4666–4672.
- [9] A. Tagliabue, A. Paris, S. Kim, R. Kubicek, S. Bergbreiter, and J. P. How, “Touch the wind: Simultaneous airflow, drag and interaction sensing on a multirotor,” *ArXiv*, vol. abs/2003.02305, 2020.
- [10] H. Seo, D. Lee, C. Y. Son, C. J. Tomlin, and H. J. Kim, “Robust trajectory planning for a multirotor against disturbance based on hamilton-jacobi reachability analysis,” in *2019 IEEE/RSJ International Conference on Intelligent Robots and Systems (IROS)*, 2020.
- [11] J. Ji, X. Zhou, C. Xu, and F. Gao, “Cmpcc: Corridor-based model predictive contouring control for aggressive drone flight,” *ArXiv*, vol. abs/2007.03271, 2020.
- [12] T. Tomić and S. Haddadin, “A unified framework for external wrench estimation, interaction control and collision reflexes for flying robots,” in *IEEE/RSJ International Conference on Intelligent Robots and Systems*, 2014.
- [13] B. Yuksel, C. Secchi, H. H. Bulthoff, and A. Franchi, “A nonlinear force observer for quadrotors and application to physical interactive tasks,” in *IEEE/ASME International Conference on Advanced Intelligent Mechatronics*, 2014.
- [14] F. Ruggiero, J. Cacace, H. Sadeghian, and V. Lippiello, “Impedance control of vtol uavs with a momentum-based external generalized forces estimator,” in *IEEE International Conference on Robotic and Automation*, 2014.
- [15] S. Kim, S. Choi, H. Kim, J. Shin, H. Shim, and H. J. Kim, “Robust control of an equipment-added multirotor using disturbance observer,” *IEEE Transactions on Control Systems Technology*, vol. 26, no. 4, pp. 1524–1531, 2018.
- [16] C. D. Mckinnon and A. P. Schoellig, “Unscented external force and torque estimation for quadrotors,” 2016.
- [17] F. Augugliaro and R. D’Andrea, “Admittance control for physical human-quadrocopter interaction,” in *Control Conference*, 2013.
- [18] A. Tagliabue, M. Kamel, S. Verling, R. Siegwart, and J. Nieto, “Collaborative object transportation using mavs via passive force control,” 2016.
- [19] D. Abeywardena, Z. Wang, G. Dissanayake, and S. L. Waslander, “Model-aided state estimation for quadrotor micro air vehicles amidst wind disturbances,” in *IEEE/RSJ International Conference on Intelligent Robots and Systems*, 2014.
- [20] S. Shen, N. Michael, and V. Kumar, “Tightly-coupled monocular visual-inertial fusion for autonomous flight of rotorcraft mavs,” in *2015 IEEE International Conference on Robotics and Automation (ICRA)*. IEEE, 2015, pp. 5303–5310.
- [21] H. J. Nussbaumer, “The fast fourier transform,” in *Fast Fourier Transform and Convolution Algorithms*. Springer, 1981, pp. 80–111.
- [22] T. Qin, S. Cao, J. Pan, and S. Shen, “A general optimization-based framework for global pose estimation with multiple sensors,” *arXiv preprint arXiv:1901.03642*, 2019.